https://doi.org/10.1016/j.ijhydene.2014.12.088 

# Numerical Investigation on Impacts on Fuel Velocity Distribution Nonuniformity among Solid Oxide Fuel Cell Unit Channels

Bin Lin[a], Yixiang Shi[a,*], Meng Ni[b,*], Ningsheng Cai[a]

[a]*Key Laboratory for Thermal Science and Power Engineering of Ministry of Education, Tsinghua University, Beijing 100084, PR China*

[b]*Building Energy Research Group, Department of Building and Real Estate, The Hong Kong Polytechnic University, Hung Hom, Kowloon, Hong Kong, PR China*

**Abstract:**

In this paper, fuel velocity distribution nonuniformity among channels in planar SOFC units under different working conditions is numerically investigated. A comprehensive three-dimensional electrochemical model is validated and then adopted in a cell unit model with structure of a real cell unit. The model couples interdependent process of species transport, heat transport, chemical reaction, electrochemical reaction, ionic conduction and electronic conduction. A nonuniformity index is proposed to quantitatively evaluate nonuniform degree of fuel velocity distribution among channels in the planar SOFC unit. The effect of the fuel velocity distribution nonuniformity on cell performance and the effects of working voltage, flow rate, flow pattern and fuel type on fuel velocity distribution nonuniformity among channels are investigated. The result shows that an increase in fuel velocity distribution nonunifomtiy can lead to a cell performance drop and fuel velocity distribution is less uniform under lower cell voltage, lower flow rate, using co-flow configuration instead of counter-flow or using syngas as fuel instead of hydrogen. In addition, the CO oxidation should be considered when studying the fuel velocity distribution nonuniformity among channels.

*Keywords:* planar solid oxide fuel cell; fuel velocity distribution among channels; nonuniformity; working condition; cell performance; modeling

**Nomenclature**

| | | | |
|---|---|---|---|
| $c$ | gas concentration (mol.m$^{-3}$) | *Greek letters* | |
| $c_p$ | molar heat capacity under constant pressure (J.mol$^{-1}$.K$^{-1}$) | $\alpha$ | transfer coefficient |

* *Corresponding author*

Key Laboratory for Thermal Science and Power Engineering of Ministry of Education, Tsinghua University, Beijing 100084, PR China. Tel.: +86 10 62789955; fax: +86 10 62789955.

E-mail address: shyx@mail.tsinghua.edu.cn (Y. Shi).

* *Corresponding author*

Building Energy Research Group, Department of Building and Real Estate, The Hong Kong Polytechnic University, Hung Hom, Kowloon, Hong Kong, PR China. Tel.: +852 27664152; fax: +852 27645131.

E-mail address: meng.ni@polyu.edu.hk (M. Ni).

| | | | |
|---|---|---|---|
| $c^*$ | concentration at equilibrium conditions ($mol.m^{-3}$) | $\beta$ | adjustable parameter |
| $D$ | gas diffusivity ($m^2.s^{-1}$) | $\varepsilon$ | porosity |
| $\Delta G$ | electrochemical reaction activation energy | $\tau$ | tortuosity factor |
| $i$ | current density ($A.m^{-2}$) | $\eta$ | overpotential (V) |
| $i_0$ | exchange current density ($A.m^{-2}$) | $\mu$ | fluid viscosity ($kg.m^{-1}.s^{-1}$) |
| $I$ | total current (A) | $\rho$ | density ($kg.m^{-3}$) |
| $j_i$ | molecular mass flux of species i ($kg.m^{-2}.s^{-2}$) | $\sigma$ | electrical conductivity ($S.m^{-1}$) |
| $k$ | coefficient of thermal conductivity ($W.m^{-1}.K^{-1}$) | $\omega_i$ | mass fraction of species i |
| $K$ | reaction equilibrium constant | $\chi_i$ | mole fraction of species i |
| $M_i$ | molecular weight of species i | *Superscript* | |
| $p$ | gas pressure (Pa) | 0 | standard state |
| $Q$ | source term of charge balance equations ($A.m^{-3}$) | eff | Effective |
| $r$ | reaction rate ($mol.m^{-2}.s^{-2}$) or radius (m) | *Subscript* | |
| $R$ | gas constant (8.314 $J.mol^{-1}.K^{-1}$) | an | Anode |
| $R_i$ | source term of mass balance equations ($kg.m^{-3}.s^{-2}$) | ca | Cathode |
| $S$ | entropy ($J.K^{-1}$) | chem | Chemistry |
| $S_{TPB}$ | TPB active area per unit volume ($m^2.m^{-3}$) | el | Electrolyte |
| $T$ | temperature (K) | elec | Electronic |
| $v$ | velocity ($m.s^{-1}$) | eq | Equilibrium |
| $V$ | voltage (V) | ion | Ionic |
| AVG | Average | inter | Interconnect |
| CV | Coefficient of Variation | prod | Product |
| PEN | Positive electrode-Electrolyte-Negative electrode | react | Reactant |
| SOFC | Solid Oxide Fuel Cell | ref | Reference |
| STD | Standard Deviation | shift | water gas shift reaction |
| TPB | Triple Phase Boundary | trans | Transfer |
| OCV | Open Circuit Voltage | | |

## 1. Introduction:

Fuel cells are electrochemical devices which can directly convert chemical energy of fuel into electricity with high efficiency and low pollutant emission [1]. Among different types of fuels cells, planar solid oxide fuel cells (SOFCs) show distinct features of fuel flexibility and potential

high power density and thus have been recognized as a promising technology for future medium-sized power generation industry [2]. However, challenges in material, cell geometry design and sealing still remain to be solved before planar SOFC commercialization [3]. One of the major challenges is the geometry design of planar interconnects. Interconnects act both as gas distributor and current collector in a planar SOFC. One aim of the interconnect optimal design is to provide a uniform fuel velocity distribution among channels on anode side to improve cell performance [4].

Many efforts have been devoted to studying the fuel velocity distribution nonuniformity among channels in planar SOFC and its influence on cell performance. Bi et al. [5] investigated numerically the effects of design parameters such as the channel height and manifold width on fuel velocity distribution nonuniformity among channels. Huang et al. [6] found experimentally that by adding small guide vines in an interconnect, the fuel velocity distribution uniformity among channels could be improved and the power density of the cell could be increased by 10%. Moreover, geometry modifications to improve fuel distribution uniformity among channels have also been proposed by researchers. Dey et al. [3] attached square type distributors on the manifolds to obtain a uniform reactant velocity distribution among channels below the active area. Liu et al. [7] adopted a symmetric bifurcation design of flow channel to gain a uniform flow field. Fuel velocity distribution nonuniformity among channels in planar SOFC unit is recognized as one crucial challenge in SOFC development.

Numerical method is essential to study fuel velocity distribution among channels inside SOFC, since SOFC is tightly sealed and it is hard to experimentally get information inside the cell such as flow velocity, temperature and gas composition. It can be time-saving and cost-effective if the numerical model can predict detailed electrode behavior and help researchers to gain a better understanding of the complex multi-physical process inside the cell. For this purpose, a reliable electrochemical model is required. However, the previous modeling studies on the fuel velocity distribution nonuniformity among channels usually focus on the transport behavior, such as fluid flow and heat transfer, while the very important electrochemical reaction kinetics are treated in a very simple manner, or even neglected.

In this paper, a comprehensive three-dimensional mechanistic model of an anode-supported SOFC unit is developed. Different from the existing models in the literature, the present model fully considers the intricate process of mass transfer, heat transfer, momentum transfer, chemical reaction, electrochemical reaction, ionic conduction and electronic conduction to predict nonuniform flow velocity distribution among channels in a SOFC unit. A validated electrochemical model is coupled with heat and momentum transfer for simulating a cell unit with real geometry. A quantitative index of nonuniformity is proposed to compare fuel velocity distribution nonuniformity among channels in different working conditions. Influence of fuel velocity nonuniformity among channels on cell performance and influence of working conditions such as working voltage, flow rate, flow pattern and fuel type on fuel velocity distribution nonuniformity among channels are studied. The results are compared with similar study.

## 2. Model development

### 2.1. Geometry and mesh

A sketch of a typical planar SOFC unit is shown in Fig. 1

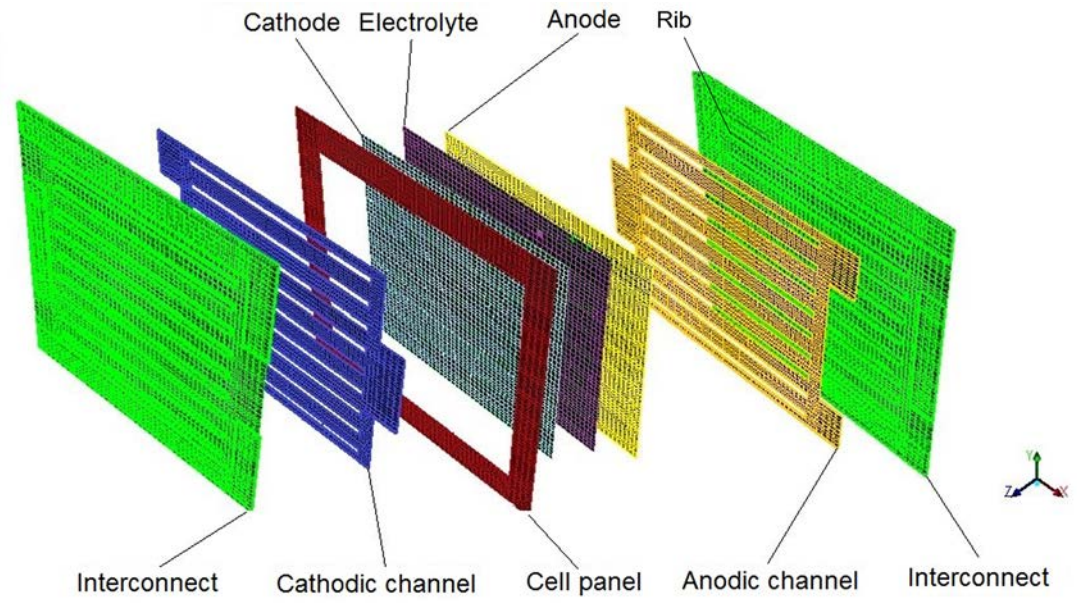


Fig.1. A sketch of a planar SOFC unit.

As can be seen from Fig.1, a typical planar SOFC unit consists of positive electrode-electrolyte-negative electrode (PEN), a cell panel for support and interconnects to distribute gas and collect current. The key geometry parameters are listed in Table 1. It should be noted that the widths of the channels are not the same. The widths of the two channels on the up and down side are 4 mm while widths of channels in the middle are 8 mm.

The mesh is refined at the anode/electrolyte interface. There are 133920 hexahedrons in the cell unit. The mesh arrangement is from a former study by Wang et al. [8]

Table 1. SOFC unit geometry

| Name | Length (mm) |
|---|---|
| PEN length | 90 |
| PEN width | 90 |
| Anode thickness | 695e-3 |
| Cathode thickness | 15e-3 |
| Electrolyte thickness | 20e-3 |
| Channel length | 80 |
| Channel height | 0.5 |
| Channel width (in the middle) | 8 |
| Channel width (on the side) | 4 |
| Rib height | 0.5 |
| Rib width | 2 |
| Interconnect thickness | 1 |

It should be noted that the channel is a cavity instead of an entity, which is created by the rib structure on interconnect.

2.2. Reactions involved

The involved reactions are listed in Table.2.

Table.2 Involved reactions

| Domain | Reactions |
|---|---|
| Anode | $H_2 + O^{2-} = H_2O + 2e^-$ |
| | $CO + O^{2-} = CO_2 + 2e^-$ |
| | $CO + H_2O \leftrightarrow CO_2 + H_2$ |
| Cathode | $O_2 + 4e^- = 2O^{2-}$ |

2.3. Model assumptions

(1) Steady state;
(2) Fuel and oxidation are approximated as ideal gases and gas mixture physical properties are estimated according to ideal gas mixing law;
(3) Ionic and electronic conductor are continuous and homogeneous, thus the reaction active sites are uniformly distributed in the electrode;
(4) Pressure gradient in the porous flow is neglected;
(5) Since the electrochemical reaction process of CO is similar to $H_2$ [9, 10]. It is assumed that the reaction kinetics of CO and $H_2$ take the same form and the only difference is the parameter value.
(6) The cell is thermally isolated from circumstance except for heat exchange at the isothermal inlets and outlets of the gas channel;
(7) All the irreversible reaction heat is generated in the anode;
(8) Radiation heat exchange between PEN and interconnects is neglected;
(9) Flow is laminar in gas channels and electrodes;
(10) Water gas shift reaction in the fuel channel is neglected;
(11) Heat convection is neglected in porous electrode;
(12) Local thermal equilibrium is assumed in the porous electrodes;

2.4. Governing equations

Considering the complexity of SOFC channel geometry, commercial CFD software Fluent™ is chosen as the simulation platform as the accuracy of the software is widely demonstrated [11]. By adding sub-routines to calculate the electric field and relevant reactions, the governing model is verified and capable of solving the multi-physical process.

2.4.1. Charge balance

The charge balance domains include anode, electrolyte, cathode and interconnects. Both oxygen ions and electrons are served as charge carriers in electrode while ions are the only conductive particles in electrolyte and electrons are the only conductive particles in interconnects. The governing equations for charge balance are summarized in Table.3.

Table.3. Governing equations for charge balance

| Domain | Governing equations | |
|---|---|---|
| Ion conservation | | |
| Anode | $-\nabla\cdot\left(\sigma_{ion,an}^{eff}\nabla V_{ion}\right)=Q_{ion,an}=i_{trans,an}S_{TPB}$ | (1) |
| Cathode | $-\nabla\cdot\left(\sigma_{ion,ca}^{eff}\nabla V_{ion}\right)=Q_{ion,ca}=-i_{trans,ca}S_{TPB}$ | (2) |
| Electrolyte | $-\nabla\cdot\left(\sigma_{ion,el}^{eff}\nabla V_{ion}\right)=Q_{ion,el}=0$ | (3) |
| Electron conservation | | |
| Anode | $-\nabla\cdot\left(\sigma_{elec,an}^{eff}\nabla V_{elec}\right)=Q_{elec,an}=-i_{trans,an}S_{TPB}$ | (4) |
| Cathode | $-\nabla\cdot\left(\sigma_{elec,ca}^{eff}\nabla V_{elec}\right)=Q_{elec,ca}=i_{trans,ca}S_{TPB}$ | (5) |
| Electrolyte | $-\nabla\cdot\left(\sigma_{elec,inter}^{eff}\nabla V_{elec}\right)=Q_{elec,inter}=0$ | (6) |

$S_{TPB}$ is the volumetric triple phase boundary (TPB) area ($m^2.m^{-3}$), which is kept a constant in the present study.

The local charge transfer current density $i_{trans,an}$ and $i_{trans,ca}$ can be formulated as [12]:

$$i_{trans,an}=i_{trans,an,H_2}+i_{trans,an,CO} \tag{7}$$

$$i_{trans,ca}=i_{trans,ca,H_2}+i_{trans,ca,CO} \tag{8}$$

$i_{trans,an,H2}$, $i_{trans,an,CO}$, $i_{trans,ca,H2}$ and $i_{trans,ca,CO}$ are local charge transfer current density in anode and cathode associated with $H_2$ and CO fuels, which can be calculated using generalized Bultler-Volmer equation as shown in equation (9):

$$i_{trans}=i_0\left(\frac{c_{react}}{c_{react}^*}\exp\left(\alpha\frac{n_eF\eta}{RT}\right)-\frac{c_{prod}}{c_{prod}^*}\exp\left(-(1-\alpha)\frac{n_eF\eta}{RT}\right)\right) \tag{9}$$

$c_{react}$, $c^*_{react}$, $c_{prod}$, $c^*_{prod}$ are reactant and product concentrations at reaction active sites and electrode/channel interface. To simplified calculation, concentration differences in products at reaction active position and electrode/gas channel interface are neglected, as shown below:

$$\frac{c_{prod}}{c_{prod}^*}=1 \tag{10}$$

According to Costamagna's study [13], the error caused by using Eq. (10) is less than 5%.

$\eta$ is local over potential, which can be obtained with equation (11):

$$\eta=V_{elec}-V_{ion}-V_{ref} \tag{11}$$

$V_{ref}$ is the potential difference between the electronic and ionic potential at the open circuit state. By setting ideal reference potential difference at anode to zero and considering the effect of gas concentration, the local overpotential for $H_2$, CO can be formulated as below:

$$\eta_{an,H_2} = V_{elec} - V_{ion} - \frac{RT}{2F}\ln\left(\frac{C_{H_2O}}{C_{H_2}}\right) \tag{12}$$

$$\eta_{an,CO} = V_{elec} - V_{ion} - \frac{RT}{2F}\ln\left(\frac{C_{CO_2}}{C_{CO}}\right) \tag{13}$$

Effects of $O_2$ concentration and temperature are considered in cathode and the overpotential can be obtained as:

$$\eta_{ca,H_2} = V_{elec} - V_{ion} - E^0_{H_2} - \frac{\Delta S^0_{H_2}}{2F}\left(T - T_0\right) - \frac{RT}{4F}\ln\left(\chi_{O_2}\right) \tag{14}$$

$$\eta_{ca,CO} = V_{elec} - V_{ion} - E^0_{CO} - \frac{\Delta S^0_{CO}}{2F}\left(T - T_0\right) - \frac{RT}{4F}\ln\left(\chi_{O_2}\right) \tag{15}$$

where $E^0_{H2}$ and $E^0_{co}$ are ideal Nernst potential and can be calculated as:

$$E^0_{H_2} = -\frac{\Delta G^0_{H_2}}{n_e F} \tag{16}$$

$$E^0_{CO} = -\frac{\Delta G^0_{CO}}{n_e F} \tag{17}$$

$i_0$ is the exchange current density, which can be formulated as below [14]:

$$i_{0,an,H_2} = \frac{\beta_{an,H_2} RT}{3F}\exp\left(-\frac{E_{act,an,H_2}}{RT}\right)\left(p_{O_2,an}\right)^{0.133} \tag{18}$$

$$i_{0,an,CO} = \frac{\beta_{an,CO} RT}{3F}\exp\left(-\frac{E_{act,an,CO}}{RT}\right)\left(p_{O_2,an}\right)^{0.133} \tag{19}$$

$$i_{0,ca,H_2} = \frac{\beta_{ca,H_2} RT}{4F}\exp\left(-\frac{E_{act,ca,H_2}}{RT}\right)\left(p_{O_2,ca}\right)^{0.25} \tag{20}$$

$$i_{0,ca,CO} = \frac{\beta_{ca,CO} RT}{4F}\exp\left(-\frac{E_{act,ca,CO}}{RT}\right)\left(p_{O_2,ca}\right)^{0.25} \tag{21}$$

$p_{O2,an}$ and $p_{O2,ca}$ are oxygen partial pressure at anode and cathode, respectively. By assuming chemical equivalence state in anode, $p_{O2,an}$ can be obtained by equation (22):

$$p_{O_2,an} = \left(\frac{p_{prod,an}}{K_{eq}\, p_{react,an}}\right)^2 \tag{22}$$

$\beta_{an,H2}$, $\beta_{an,CO}$, $\beta_{ca,H2}$, $\beta_{ca,CO}$ and $\tau$ are the adjustable parameters for fitting the experimental data.

2.4.2 Mass balance

The mass balance domains include anode, cathode and gas channels. In anode, electrochemical reactions for $H_2$ and CO as well as water gas shift reactions are considered while only electrochemical reaction for $O_2$ is considered in cathode. Since water gas shift reaction is neglected in the fuel channel, there is no mass source term in gas channels. The governing equations for mass balance are summarized in Table.4.

Table.4. Governing equations for mass balance

| Domain | Governing equations | |
|---|---|---|
| Anode | $\nabla\left(\rho_{fuel}\vec{v}x_{H_2}-\rho_{fuel}\omega_{H_2}\sum_{k=1}^{N}D_{H_2,k}^{eff}\nabla x_k\right)=R_{H_2}=-\frac{i_{trans,an,H_2}S_{TPB}M_{H_2}}{2F}+r_{shift}M_{H_2}$ | (23) |
| | $\nabla\left(\rho_{fuel}\vec{v}x_{H_2O}-\rho_{fuel}\omega_{H_2O}\sum_{k=1}^{N}D_{H_2O,k}^{eff}\nabla x_k\right)=R_{H_2O}=\frac{i_{trans,an,H_2}S_{TPB}M_{H_2O}}{2F}-r_{shift}M_{H_2O}$ | (24) |
| | $\nabla\left(\rho_{fuel}\vec{v}x_{CO}-\rho_{fuel}\omega_{CO}\sum_{k=1}^{N}D_{CO,k}^{eff}\nabla x_k\right)=R_{CO}=-\frac{i_{trans,an,CO}S_{TPB}M_{CO}}{2F}-r_{shift}M_{CO}$ | (25) |
| | $\nabla\left(\rho_{fuel}\vec{v}x_{CO_2}-\rho_{fuel}\omega_{CO_2}\sum_{k=1}^{N}D_{CO_2,k}^{eff}\nabla x_k\right)=R_{CO_2}=\frac{i_{trans,an,CO}S_{TPB}M_{CO_2}}{2F}+r_{shift}M_{CO_2}$ | (26) |
| | $\nabla\left(\rho_{fuel}\vec{v}\right)=R_{H_2}+R_{H_2O}+R_{CO}+R_{CO_2}$ | (27) |
| Cathode | $\nabla\left(\rho_{air}\vec{v}x_{O_2}-\rho_{air}\omega_{H_2}\sum_{k=1}^{N}D_{O_2,k}^{eff}\nabla x_k\right)=R_{O_2}=\frac{i_{trans,ca}S_{TPB}M_{O_2}}{4F}$ | (28) |
| | $\nabla\left(\rho_{air}\vec{v}\right)=R_{O_2}$ | (29) |
| Anodic channel | $\nabla\left(\rho_{fuel}\vec{v}x_{H_2}-\rho_{fuel}\omega_{H_2}\sum_{k=1}^{N}D_{H_2,k}^{eff}\nabla x_k\right)=0$ | (30) |
| | $\nabla\left(\rho_{fuel}\vec{v}x_{H_2O}-\rho_{fuel}\omega_{H_2O}\sum_{k=1}^{N}D_{H_2O,k}^{eff}\nabla x_k\right)=0$ | (31) |
| | $\nabla\left(\rho_{fuel}\vec{v}x_{CO}-\rho_{fuel}\omega_{H_2}\sum_{k=1}^{N}D_{CO,k}^{eff}\nabla x_k\right)=0$ | (32) |
| | $\nabla\left(\rho_{fuel}\vec{v}x_{CO_2}-\rho_{fuel}\omega_{H_2}\sum_{k=1}^{N}D_{CO_2,k}^{eff}\nabla x_k\right)=0$ | (33) |
| | $\nabla\left(\rho_{fuel}\vec{v}\right)=0$ | (34) |

| | | |
|---|---|---|
| Cathodic channel | $\nabla\left(\rho_{air}\vec{v}x_{O_2}-\rho_{air}\omega_{O_2}\sum_{k=1}^{N}D_{O_2,k}^{eff}\nabla x_k\right)=0$ | (35) |
| | $\nabla\left(\rho_{air}\vec{v}\right)=0$ | (36) |

As can be seen from Table.4, gas diffusion in porous electrodes is described by Fick's law. $D^{eff}_{i,k}$ is the effective diffusivity between specie *i* and *k*. In this paper, $D^{eff}_{i,k}$ is approximated as a function of electrode porosity, tortuosity factor and binary diffusion coefficient [15], which can be determined using expression by Fuller et al. [16]:

$$D_{i,k}^{eff}=\frac{\varepsilon}{\tau}D_{i,k}=\frac{\varepsilon}{\tau}\frac{0.00143T^{1.75}}{pM_{ik}^{1/2}\left[V_i^{1/3}+V_k^{1/3}\right]^2} \tag{37}$$

where ε is the electrode porosity and τ is the tortuosity factor. By adjusting the value of τ, effects of Knudsen diffusion and surface diffusion in the porous electrode are included in the diffusion model. Obviously, ε/τ is equal to 1 in the channels.
where

$$M_{ik}=2\left[\left(1/M_i\right)+\left(1/M_k\right)\right]^{-1} \tag{38}$$

here $M_i$ and $M_k$: molar mass of specie *i* and *k*; $V_i$ and $V_k$: special Fuller diffusion volume. The expression for $D_{i,k}$ is simplified as a linearized function of temperature in the simulation process.

$r_{shift}$ is the reaction rate of water gas shift reaction and can be formulated as below [17]:

$$r_{shift}=k_{shift}\left(p_{H_2O}p_{CO}-\frac{p_{H_2}p_{CO_2}}{K_{shift}}\right) \tag{39}$$

where $K_{shift}$ is the equilibrium constant of water gas shift reaction and can be formulated as below :

$$K_{shift}=\exp\left(-0.2935Z^3+0.6351Z^2+4.1788Z+0.3169\right) \tag{40}$$

where

$$Z=\frac{1000}{T}-1 \tag{41}$$

$k_{shift}$ is the reaction rate of water gas shift reaction and can be formulated as below:

$$k_{shift}=0.0171\exp\left(-\frac{103191}{RT}\right) \tag{42}$$

2.4.3. Momentum balance

In gas channels, the laminar flow is described by the Navier-Stokes equation, while flow in porous electrodes is described by Darcy's law. The governing equations are listed in Table.5.

Table.5. Governing equations for momentum balance

| Domain | Governing equations | |
|---|---|---|
| Electrodes | $\nabla\cdot\left(\varepsilon\rho_{gas}\vec{v}\vec{v}\right)=-\varepsilon\nabla p+\nabla\left[\varepsilon\mu_{gas}\left(\nabla\vec{v}+\left(\nabla\vec{v}\right)^{T}\right)\right]-\frac{\mu_{gas}}{\alpha}\varepsilon^{2}\vec{v}$ | (43) |
| Channels | $\nabla\cdot\left(\rho_{gas}\vec{v}\vec{v}\right)=-\nabla p+\nabla\left[\mu_{gas}\left(\nabla\vec{v}+\left(\nabla\vec{v}\right)^{T}\right)\right]$ | (44) |

2.4.4. Energy balance

Since radiative heat transfer is neglected in the model, the heat is conducted only via heat conduction and heat convection. Heat source results from three parts: chemical reaction heat, electrochemical reaction heat and ohmic heat. The governing equation for all domains are shown in Table.6.

Table.6. Governing equations for energy balance

| Domain | Governing equations | |
|---|---|---|
| Anode | $\nabla\cdot\left(-k\nabla T\right)=r_{shift}T\left(S_{H_2}+S_{CO_2}-S_{H_2O}-S_{CO}\right)+\frac{R_{H_2,an}T\left(S_{H_2O}-\frac{1}{2}S_{O_2}-S_{H_2}\right)}{M_{H_2}}+\frac{R_{CO,an}T\left(S_{CO_2}-\frac{1}{2}S_{O_2}-S_{CO}\right)}{M_{CO}}+\eta_{an,H_2}\left\lvert Q_{elec.an,H_2}\right\rvert+\eta_{an,CO}\left\lvert Q_{elec.an,CO}\right\rvert+\frac{i_{ion}^{2}}{\sigma_{an,ion}}+\frac{i_{elec}^{2}}{\sigma_{an,elec}}$ | (45) |
| Cathode | $\nabla\cdot\left(-k\nabla T\right)=\eta_{ca}\left\lvert Q_{elec.ca}\right\rvert+\frac{i_{ion}^{2}}{\sigma_{an,ion}}+\frac{i_{elec}^{2}}{\sigma_{an,elec}}$ | (46) |
| Electrolyte | $\nabla\cdot\left(-k\nabla T\right)=\frac{i_{ion}^{2}}{\sigma_{el,ion}}$ | (47) |
| Interconnects | $\nabla\cdot\left(-k\nabla T\right)=\frac{i_{elec}^{2}}{\sigma_{inter,elec}}$ | (48) |
| Channels | $\nabla\cdot\left(-k\nabla T+\vec{v}\cdot\rho c_{p}T\right)=0$ | (49) |

It should be noted that the heat sources are reduced to 10% to accelerate the simulation process.

2.5. Parameter settings

The material parameters are listed in Table.7.

In this paper, the cell panel uses the same material as the interconnects.

Table.7. Material properties [18]

| | Cathode | Electrolyte | Anode | Interconnects |
|---|---|---|---|---|
| Material | LSM-ScSZ | YSZ | Ni-YSZ | Mg doped $LaCrO_3$ |
| Effective ionic conductivity, $\sigma_{ion}\left(S.m^{-1}\right)$ | $6.92\times10^{4}\exp\left(-\frac{9681}{T}\right)(1-\varepsilon)$ | $3.34\times10^{4}\exp\left(-\frac{10300}{T}\right)$ | $(0.002T-1.4483)(1-\varepsilon)$ | - |
| Effective electronic conductivity, $\sigma_{elec}\left(S.m^{-1}\right)$ | $\frac{4.2\times10^{7}}{T}\exp(1150/T)(1-\varepsilon)$ | - | $\left(3.27\times10^{6}-1065.3T\right)(1-\varepsilon)$ | $\frac{9.3\times10^{6}}{T}\exp\left(-\frac{1100}{T}\right)$ |
| Porosity, $\varepsilon$ | 0.365 | - | 0.365 | - |
| Specified heat capacity $c_p\left(J.kg^{-1}.K^{-1}\right)$ | 390 | 300 | 420 | 444 |
| Density $\rho\left(kg.m^{-3}\right)$ | 6570 | 2000 | 6870 | 8900 |
| Thermal conductivity $k\left(W.m^{-1}.K^{-1}\right)$ | 9.6 | 2.7 | 6.23 | 30 |

2.6. Sub-model validation

By specifying corresponding source terms and diffusion coefficients in Fluent™, the governing equations of the model can be incorporated into Fluent and solved.

A button cell using hydrogen and syngas as fuel is simulated and the result is compared with the corresponding experiment data to validate the electrochemical model.

Average current density in electrolyte at a specified cell voltage is calculated and compared with corresponding experimental data. Considering the current distribution, the average current density can be obtained using equation as below [19]:

$$i_{avg}=\frac{1}{S_{ca}}I_{total}=\frac{1}{\pi R_{ca}^{2}}\int_{0}^{R_{el}}2\pi r i_{local}dr \tag{50}$$

where $i_{avg}$ is the average ionic current density. By changing cell voltage over and calculate corresponding $i_{avg}$, a full polarization curve can be obtained.

The adjustable parameters include $\beta_{an,H2}$, $\beta_{an,CO}$, $\beta_{ca,H2}$, $\beta_{ca,CO}$ and τ. Their values are adjusted to fit the simulated polarization curve with experimental data. The values of adjustable parameters are listed in Table.8.

It should be noted that the ratios of the adjustable parameters on the same fuel were kept as constants from literature [19] in the validation process.

Table.8. Adjustable model parameters

| Fuel type | Parameter | Value |
|---|---|---|

| | | |
|---|---|---|
| | Adjustable parameter, $\beta_{an,H_2}$ | $2\times10^{10}$ |
| | Adjustable parameter, $\beta_{an,CO}$ | $5\times10^{9}$ |
| syngas | | |
| | Adjustable parameter, $\beta_{ca,H_2}$ | $2\times10^{8}$ |
| | Adjustable parameter, $\beta_{ca,CO}$ | $5\times10^{7}$ |
| | Adjustable parameter, $\beta_{an,H_2}$ | $6\times10^{10}$ |
| hydrogen | | |
| | Adjustable parameter, $\beta_{ca,H_2}$ | $6\times10^{8}$ |
| electrode | $\tau$ | 7 |

Then, by varying the operating temperature while keeping adjustable parameter constants, polarization curves at different temperatures can be obtained.

In the validation process, the cell voltage is varied from 0.3V to 1.0V, which is a usual range for a cell unit working voltage.

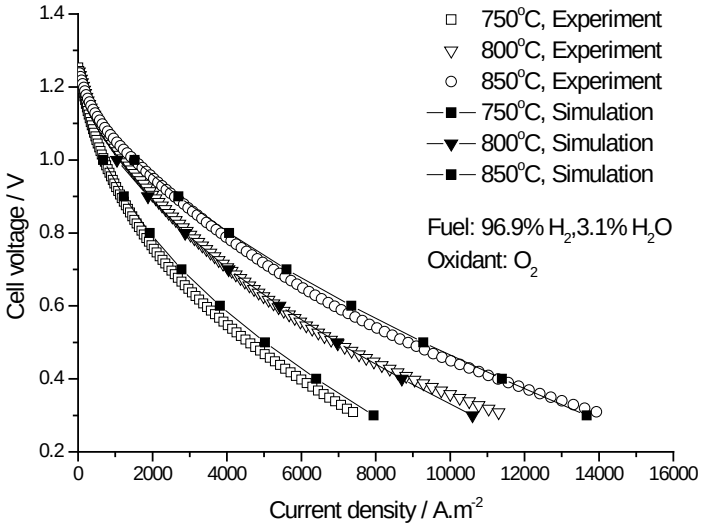


Fig.2. Model validation using hydrogen as fuel at different temperatures.

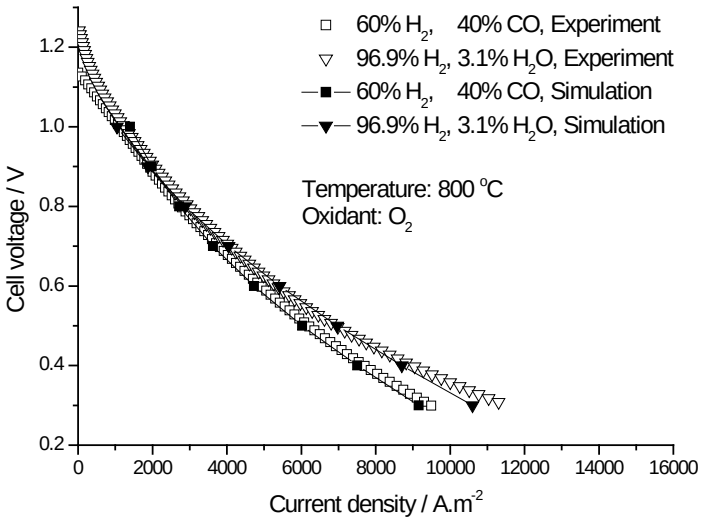


Fig.3. Model validation using hydrogen and syngas as fuel at the same temperature.

As can been seen from Fig.2 and Fig.3, the simulation results are in good agreement with the experimental data, especially when cell voltage is between 0.3V and 0.9V, where the biggest error is less than 11%.

2.7. Nonuniformity index

To quantitatively evaluate and compare degrees of fuel velocity distribution nonuniformity among channels in a planar SOFC unit, a nonuniformity index is required. In this paper, the coefficient of variation of velocity magnitudes at the centers of each channel inlet is adopted as the nonuniformity index. Coefficient of variation (*CV*) is a dimensionless number which measures dispersion of a distribution and is capable of comparing dispersion degrees of distributions with different mean values. The definition of coefficient of variation is shown below:

$$CV = \frac{STD}{\frac{1}{n}\sum_{i=1}^{n} u_i} \tag{51}$$

where $u_i$ is the velocity magnitude at the center of channel $i$. $n$ is the total number of the channels concerned. For the 10-channel interconnect in this paper:

$$n = 10 \tag{52}$$

*STD* is the standard deviation of $u_i$, defined as:

$$STD = \left( \frac{1}{n}\sum_{i=1}^{n}\left( u_i - \frac{1}{n}\sum_{i=1}^{n} u_i \right)^2 \right)^{\frac{1}{2}} \tag{53}$$

**3. Result and discussion**

Degrees of fuel velocity distributions nonuniformity among channels in different cases are obtained and compared. The effect of fuel velocity distribution nonuniformity among channels on cell performance and the effects of reaction, working voltage, flow rate, flow pattern and fuel composition on fuel velocity distribution nonuniformity are investigated.

### 3.1 Base case simulation result

#### 3.1.1 Operating condition

Operating conditions in base case are listed in Table.9.

Table.9. Operating conditions in base case

| Parameters | Value |
|---|---|
| Pressure (Pa) | 101325 |
| Fuel inlet temperature (K) | 1073 |
| Oxidant inlet temperature (K) | 1073 |
| Fuel mole percentage | 60%$H_2$, 40%CO |
| Oxidant mole percentage | 21%$O_2$, 79%$N_2$ |
| Fuel inlet mass flow rate (kg.s$^{-1}$) | 9.87e-7 (0.2 m.s$^{-1}$) |
| Oxidant inlet mass flow rate (kg.s$^{-1}$) | 6.89e-6 (0.6 m.s$^{-1}$) |
| Working voltage (V) | 0.8 |

#### 3.1.2 Fuel velocity magnitude distribution

Fig.4 shows the velocity magnitude distribution in the anodic channel. The fuel enters the anodic channel from the single inlet on the left, flows across 10 channels and leaves the fuel channel through two outlets on the right. It can be seen that the velocity magnitude increases along flow direction. The highest velocity appears at the corner of the outlets. It can also be observed from Fig.4 that the fuel velocity distribution among the channels is not uniform.

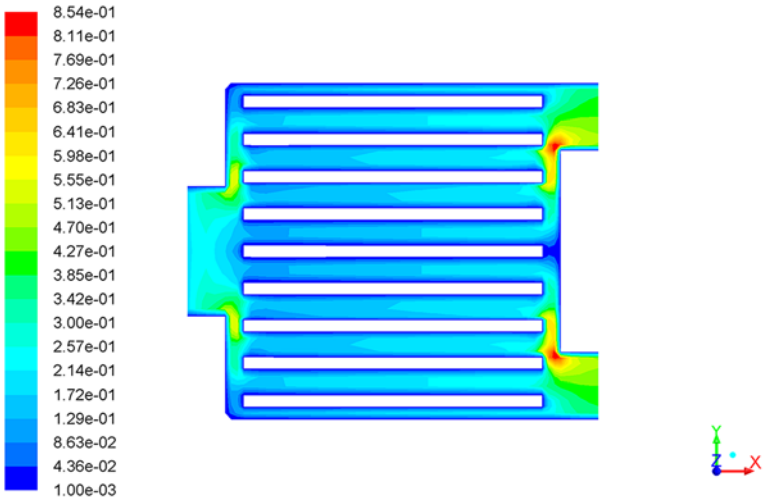


Fig.4. Velocity magnitude distribution in anodic channel.

Fig.5 shows the distribution of velocity magnitudes at the centers of rectangle channel inlets. The channels are numbered from 1 to 10 along the positive Y axis in Fig.4. The velocity distribution is symmetrical and the highest velocities appear in channel 3 and 8. The nonuniformity index *CV* of the base case is 0.1570.

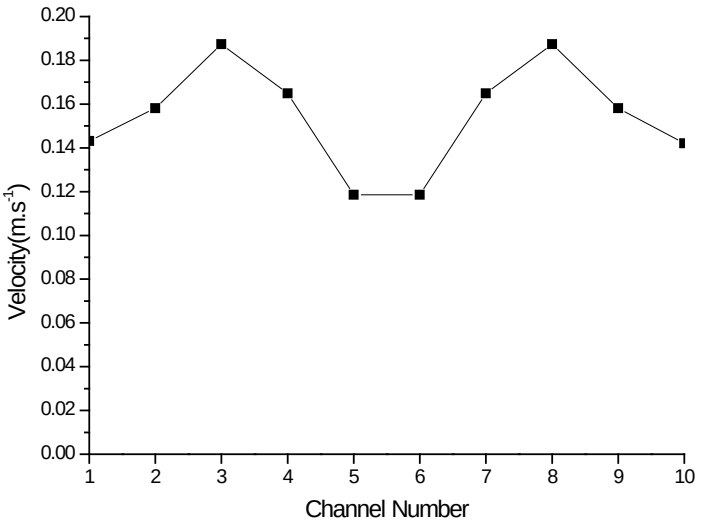


Fig.5. Center fuel velocity magnitude distribution.

3.1.3 Species distribution

Fig.6 shows the mole fraction distribution of specie $H_2$, $H_2O$, CO and $CO_2$. As can be seen, the mole fraction of $H_2$ decreases along the channel due to the electrochemical consumption. The mole distribution of CO is similar to $H_2$ while mole fraction of $H_2O$ and $CO_2$ increase monotonically along the channel. The specie distributions are affected by the nonuniform fuel distribution: higher fuel velocity in channel 3 and 8 leads to the higher reactant mole fraction and lower product mole fraction. The consumption rates of the reactants and the formation rates of the products are different in each channel due to the nonuniform fuel velocity distribution among channels. The fuel utilization rate for $H_2$ and CO are 39.6% and 74.1%, respectively. The higher fuel utilization rate for CO could be attributed to the water gas shift reaction.

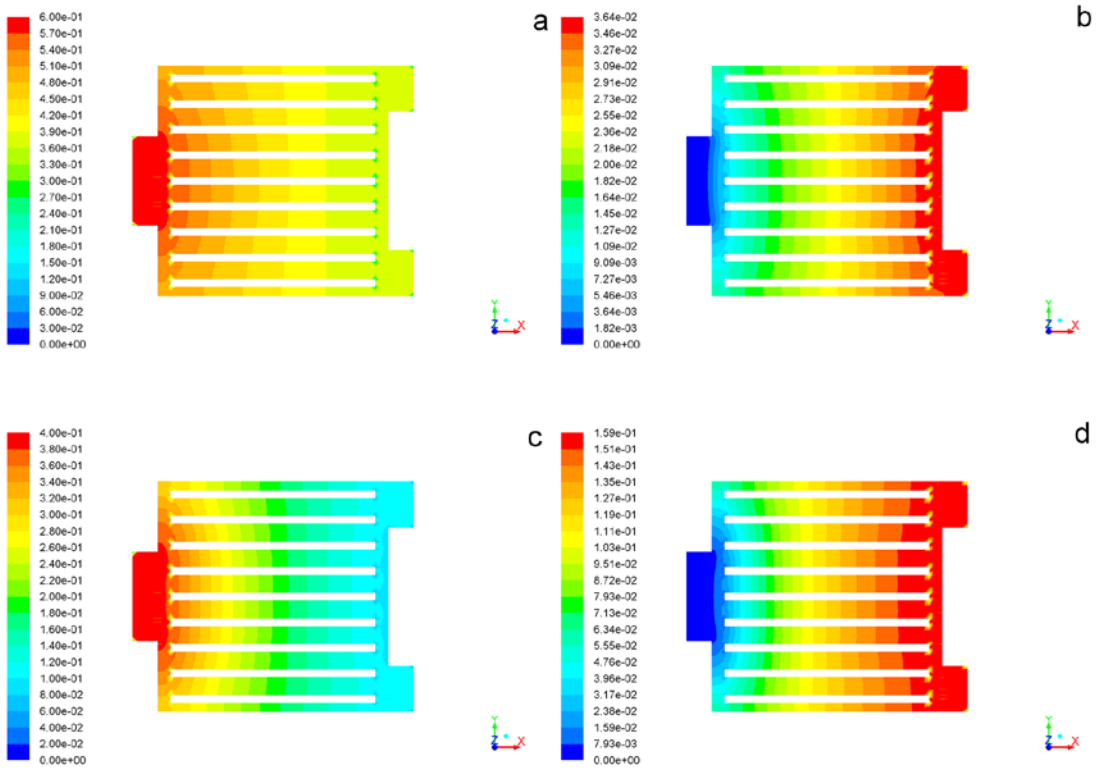


Fig.6. Specie distributions in the anodic channel: (a) Mole fraction of $H_2$; (b) Mole fraction of $H_2O$; (c) Mole fraction of CO; (d) Mole fraction of $CO_2$.

3.1.4 Current density distribution

Fig.7 is the current density distribution in the middle section of the electrolyte. It can be seen from Fig.7 that the current density is different in the electrolyte region over different channels due to the nonuniform fuel velocity distribution among channels. Higher fuel velocity in channel 3 and 8 side leads to higher current density. It is also shown in the figure that current density in region over fuel channels is higher than the region over center line interconnect ribs, which can be explained by the low fuel concentration in the anode region over anode/interconnect interface due to large diffusion resistance. It should be noted that the highest current density appears in the region above the edge of interconnects upstream since the current collection and gas diffusion are both easier in this region. On the other hand, current density is higher in the electrolyte region over upstream anodic channel, since the fuel concentration is higher in the region. The average current density in the electrolyte is 567 $A.m^{-2}$ which is only 21% of the current density in button cell under the same voltage. The reason is the low fuel concentration in anode region over the interconnect downstream. The low fuel concentration can actually increase the anode reference potential difference, which in turn yields lower local current density.

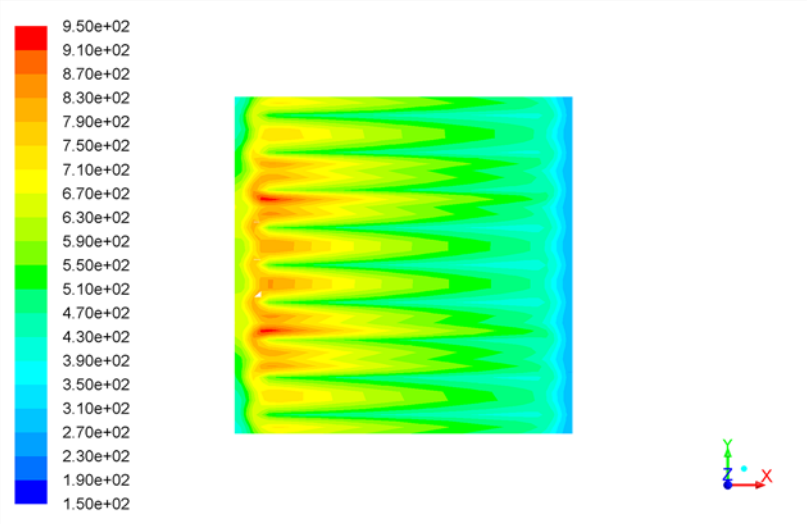


Fig.7. Current density in the middle section of the electrolyte

3.1.5 Temperature distribution

Fig.8 shows the temperature distribution on the cathodic interconnect. As can be seen, the temperature is lower near the air entrance since the major cooling source for the cell unit is the excess air. Also, the temperature of the region near fuel inlet is lower than of the surrounding region. The temperature difference in Y direction is due to the nonuniform fuel velocity distribution among channels. In the middle region of the interconnect, higher fuel velocity in channel 3 and 8 leads to higher temperature. The largest temperature gradient appears in the region near cathodic channel inlet. The maximum temperature gradient in the interconnect is 436 $K.m^{-1}$.


Fig.8. Temperature distribution on the cathodic interconnect

3.2 Effect of fuel distribution nonuniformity on cell performance

To investigate the effect of fuel velocity distribution nonuniformity among channels on cell

performance, a contracting case with one anodic channel outlet blocked is studied.

The fuel velocity distribution of the base case and the contracting case is shown in Fig.9. As can be seen from the Fig.9, the fuel velocity distribution becomes less uniform when blocking one anodic channel outlet due to the velocity drop of the channels close to the blocked outlet and the velocity increase of the channels close to the unblocked outlet.

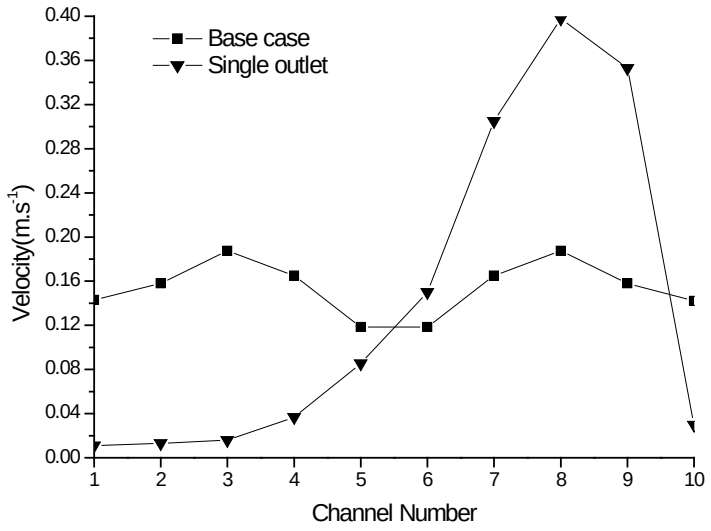


Fig.9. Center fuel velocity magnitude distribution for cell units with different flow field structure.

Since other working conditions such as working voltage and flow rate are kept the same, the effect of the fuel distribution nonuniformity can be obtained by comparing case 0 and base case. The result is shown in Table.10.

Table.10. Contrasting cases with different flow field structure

| Parameters | Base case | Case 0 (Single outlet) |
|---|---|---|
| Fuel mole percentage | 60%$H_2$,40%CO | 60%$H_2$,40%CO |
| Oxidant mole percentage | 21%$O_2$, 79%$N_2$ | 21%$O_2$, 79%$N_2$ |
| Fuel inlet mass flow rate ($kg.s^{-1}$) | 9.87e-7 (0.2 m/s) | 9.87e-7 (0.2 m/s) |
| Oxidant inlet mass flow rate ($kg.s^{-1}$) | 6.89e-6 (0.6 m/s) | 6.89e-6 (0.6 m/s) |
| Cell voltage (V) | 0.8 | 0.8 |
| Average current density in electrolyte ($A.m^{-2}$) | 567 | 535 |
| Fuel utilization rate | $H_2$:39.6%; CO:74.1% | $H_2$:36.8%; CO:69.6% |
| $\nabla T_{inter,\ MAX}$ ($K.m^{-1}$) | 436 | 743 |
| STD ($m.s^{-1}$) | 0.0242 | 0.1539 |
| AVG ($m.s^{-1}$) | 0.1543 | 0.1397 |
| CV | 0.1570 | 1.1010 |

As can be seen from Table.10, CV in case 0 is 7 times higher than in base case, indicating a significant increase in fuel velocity distribution nonuniformity among channels. The fuel

distribution nonuniformity increase leads to 5.6% decrease in average current density as well as 2.8% and 4.5% decrease in fuel utilization rate for $H_2$ and CO, respectively. Also, the more nonuniform fuel flow field leads to a higher maximum local temperature gradient and thus higher maximum local thermal stress, which may shorten SOFC unit life in the long-term operation.

3.3 Fuel velocity distribution nonuniformity among channels in different working conditions

To study the effects of reaction, working voltage, flow pattern, flow rate and fuel type on fuel velocity distribution nonuniformity among channels, sets of contrasting cases are investigated. By comparing nonuniformity indexes of the contrasting cases, factors which may affect the fuel velocity distribution nonuniformity among channels are identified and discussed.

3.3.1 Effect of reaction on fuel velocity distribution nonuniformity among channels

A cell unit using the same fuel as in base case but has no reaction is simulated and compared with base case, as shown in Table.11:

Table.11. Contrasting cases with and without reaction

| Parameters | Base case | Case 1 (no reaction) |
|---|---|---|
| Fuel mole percentage | 60%$H_2$,40%CO | 60%$H_2$,40%CO |
| Oxidant mole percentage | 21%$O_2$, 79%$N_2$ | 21%$O_2$, 79%$N_2$ |
| Fuel inlet mass flow rate ($kg.s^{-1}$) | 9.87e-7 (0.2 $m.s^{-1}$) | 9.87e-7 (0.2 $m.s^{-1}$) |
| Oxidant inlet mass flow rate ($kg.s^{-1}$) | 6.89e-6 (0.6 $m.s^{-1}$) | 6.89e-6 (0.6 $m.s^{-1}$) |
| Cell voltage (V) | 0.8 | - |
| Average current density in electrolyte ($A.m^{-2}$) | 567 | 0 |
| Fuel utilization rate | $H_2$:39.6%; CO:74.1% | 0 |
| $\nabla T_{inter,\ MAX}$ ($K.m^{-1}$) | 436 | 0 |
| STD ($m.s^{-1}$) | 0.0242 | 0.0221 |
| AVG ($m.s^{-1}$) | 0.1543 | 0.1538 |
| CV | 0.1570 | 0.1434 |

All parameters in case 1 are kept the same with in base case except that no reaction is considered.

*CV* in base case is larger than in case 1, indicating that the reaction will increase fuel velocity distribution nonuniformity among channels in a cell unit.

3.3.2 Effect of working voltage on fuel velocity distribution nonuniformity among channels

Cell units with different cell voltages are simulated and compared, as shown in Table.12:

Table.12. Contrasting cases with different cell voltage

| Parameters | Case 2 | Base case | Case 3 |
|---|---|---|---|
| Fuel mole percentage | 60%$H_2$,40%CO | 60%$H_2$,40%CO | 60%$H_2$,40%CO |

| | | | |
|---|---|---|---|
| Oxidant mole percentage | 21%$O_2$, 79%$N_2$ | 21%$O_2$, 79%$N_2$ | 21%$O_2$, 79%$N_2$ |
| Fuel inlet mass flow rate ($kg.s^{-1}$) | 9.87e-7 (0.2 $m.s^{-1}$) | 9.87e-7 (0.2 $m.s^{-1}$) | 9.87e-7 (0.2 $m.s^{-1}$) |
| Oxidant inlet mass flow rate ($kg.s^{-1}$) | 6.89e-6 (0.6 $m.s^{-1}$) | 6.89e-6 (0.6 $m.s^{-1}$) | 6.89e-6 (0.6 $m.s^{-1}$) |
| Cell voltage (V) | 0.7 | 0.8 | 0.9 |
| Average current density in electrolyte ($A.m^{-2}$) | 892 | 567 | 318 |
| Fuel utilization rate | $H_2$:47.2%; CO:89.8% | $H_2$:39.6%; CO:74.1% | $H_2$:35.0%; CO:55.5% |
| $\nabla T_{inter,\ MAX}$ ($K.m^{-1}$) | 678 | 436 | 320 |
| STD ($m.s^{-1}$) | 0.0287 | 0.0242 | 0.0223 |
| AVG ($m.s^{-1}$) | 0.1588 | 0.1543 | 0.1532 |
| CV | 0.1805 | 0.1570 | 0.1459 |

Cell voltage in case 2 is lower than in base case while cell voltage in case 3 is higher. As can be observed from Table.12, average current density and fuel utilization rates for both $H_2$ and CO increase with decreasing cell voltage. Higher *CV* value in lower cell voltage condition suggests a less uniform fuel velocity distribution among channels while larger maximum temperature gradient suggests a larger maximum local thermal stress.

3.3.3 Effect of flow rate on fuel velocity distribution nonuniformity among channels

Cell units with different flow rates are simulated and compared, as shown in Table.13:

Table.13. Contrasting cases with different flow rates

| Parameters | Case 4 | Base case | Case 5 |
|---|---|---|---|
| Fuel mole percentage | 60%$H_2$,40%CO | 60%$H_2$,40%CO | 60%$H_2$,40%CO |
| Oxidant mole percentage | 21%$O_2$, 79%$N_2$ | 21%$O_2$, 79%$N_2$ | 21%$O_2$, 79%$N_2$ |
| Fuel inlet mass flow rate ($kg.s^{-1}$) | 7.90e-7 (0.16 $m.s^{-1}$) | 9.87e-7 (0.2 $m.s^{-1}$) | 1.18e-6 (0.24 $m.s^{-1}$) |
| Oxidant inlet mass flow rate ($kg.s^{-1}$) | 5.51e-6 (0.48 $m.s^{-1}$) | 6.89e-6 (0.6 $m.s^{-1}$) | 8.27e-6 (0.72 $m.s^{-1}$) |
| Cell voltage (V) | 0.8 | 0.8 | 0.8 |
| Average current density in electrolyte ($A.m^{-2}$) | 524 | 567 | 603 |
| Fuel utilization rate | $H_2$:44.2%; CO:80.5% | $H_2$:39.6%; CO:74.1% | $H_2$:35.6%; CO:68.4% |
| $\nabla T_{inter,\ MAX}$ ($K.m^{-1}$) | 385 | 436 | 484 |
| STD ($m.s^{-1}$) | 0.0209 | 0.0242 | 0.0285 |
| AVG ($m.s^{-1}$) | 0.1219 | 0.1543 | 0.1874 |
| CV | 0.1715 | 0.1570 | 0.1518 |

Flow rates of fuel and oxidant in case 4 are about 80% of the flow rates in base case while flow rates in case 5 are 120%. It can be seen from Table.13 that with the increasing flow rates, average current density in electrolyte increases while fuel utilization rates for both $H_2$ and CO

decrease. With increasing flow rates, STD increases but CV decreases, which suggests that absolute dispersion of the velocity increases but relative dispersion decreases. Since relative flow rate difference is more concerned in this paper, the fuel velocity distribution among channels is thought to be less uniform with lower flow rates. In addition, the maximum temperature gradient increases with increasing flow rates, indicating a larger maximum local thermal stress in interconnect.

3.3.4 Effect of flow pattern on fuel velocity distribution nonuniformity among channels

A co-flow SOFC unit with the opposite fuel flow direction from base case is simulated and compared with base case and the result is shown in Table.14:

Table.14. Contrasting cases with and without reaction

| Parameters | Base case (counter-flow) | Case 6 (co-flow) |
|---|---|---|
| Fuel mole percentage | 60%$H_2$,40%CO | 60%$H_2$,40%CO |
| Oxidant mole percentage | 21%$O_2$, 79%$N_2$ | 21%$O_2$, 79%$N_2$ |
| Fuel inlet mass flow rate ($kg.s^{-1}$) | 9.87e-7 | 2×4.935e-7 |
| Oxidant inlet mass flow rate ($kg.s^{-1}$) | 6.89e-6 | 6.89e-6 |
| Cell voltage (V) | 0.8 | 0.8 |
| Average current density in electrolyte ($A.m^{-2}$) | 567 | 560 |
| Fuel utilization rate | $H_2$:39.6%; CO:74.1% | $H_2$:39.6%; CO:73.6% |
| $\nabla T_{inter,\,MAX}$ ($K.m^{-1}$) | 436 | 379 |
| STD ($m.s^{-1}$) | 0.0242 | 0.0284 |
| AVG ($m.s^{-1}$) | 0.1543 | 0.1028 |
| CV | 0.1570 | 0.2758 |

All parameters in case 6 are kept the same with in base case except for the opposite fuel flow direction.

As can be seen from Table.14, in the co-flow case, the fuel velocity distribution among channels is less uniform and the current density is 1.25% lower than in the counter-flow case. However, the counter-flow SOFC unit might suffer from a larger maximum local thermal stress, since the maximum temperature gradient is 15% higher than in the co-flow case.

3.3.5 Effect of fuel types on fuel velocity distribution nonuniformity among channels

A cell unit using hydrogen as fuel is simulated and compared with base case, as shown in Table.15:

Table.15. Contrasting cases using different fuels

| Parameters | Base case | Case 7 |
|---|---|---|
| Fuel mole percentage | 60%$H_2$,40%CO | 96.9%$H_2$,3.1%$H_2O$ |
| Oxidant mole percentage | 21%$O_2$, 79%$N_2$ | 21%$O_2$, 79%$N_2$ |
| Fuel inlet mass flow rate ($kg.s^{-1}$) | 9.87e-7 (0.2 $m.s^{-1}$) | 2.00e-7 (0.2 $m.s^{-1}$) |

| | | |
|---|---|---|
| Oxidant inlet mass flow rate ($kg.s^{-1}$) | 6.89e-6 (0.6 $m.s^{-1}$) | 6.89e-6 (0.6 $m.s^{-1}$) |
| Cell voltage (V) | 0.8 | 0.8 |
| Average current density in electrolyte ($A.m^{-2}$) | 567 | 604 |
| Fuel utilization rate | $H_2$:39.6%; CO:74.1% | $H_2$:29.5% |
| $\nabla T_{inter,\,MAX}$ ($K.m^{-1}$) | 436 | 365 |
| STD ($m.s^{-1}$) | 0.0242 | 0.0186 |
| AVG ($m.s^{-1}$) | 0.1543 | 0.1236 |
| CV | 0.1570 | 0.1504 |

$H_2$ is used as fuel in case 7 and the fuel mass flow rate is adjusted to ensure the same fuel inlet velocity as in base case while other conditions remain the same. Table.15 shows that, average current density in case 7 is higher than in base case. Moreover, *CV* value and maximum temperature gradient are lower in case 7, which indicate a less nonuniform fuel velocity distribution among channels and smaller maximum local thermal stress.

3.3.6 Comparison with similar work

Huang et al [4] have done similar research on fuel velocity distribution nonuniformity among channels with different interconnects and in different working conditions.

The degree of fuel velocity nonuniformity among channels is measure by percentage of uniformity, which is defined as:

$$Percentage\ of\ Uniformity = 1 - \left( \frac{1}{n} \sum_{i=1}^{n} \left( \frac{u_i - \frac{1}{n} \sum_{i=1}^{n} u_i}{\frac{1}{n} \sum_{i=1}^{n} u_i} \right)^2 \right)^{\frac{1}{2}} = 1 - CV \tag{54}$$

where $u_i$ is the fuel velocity of channel *i*. *n* is the total number of the channels concerned.

The similar nonuniformity index makes the simulation result comparable with in this paper. Huang neglects the electrochemical oxidation of CO and only considers water gas shift reaction and $H_2$ electrochemical oxidation. The result shows that the percentage of uniformity decreases with increasing flow rates, which is opposite to the conclusion in this subsection 3.3.3.

To study the effect of CO oxidation on the change of percentage of uniformity against fuel flow rate, contracting cases with and without CO oxidation are studied. The flow rates are kept the same as in subsection 3.3.3. The results of the contracting cases and Huang's work are shown in Fig.10.

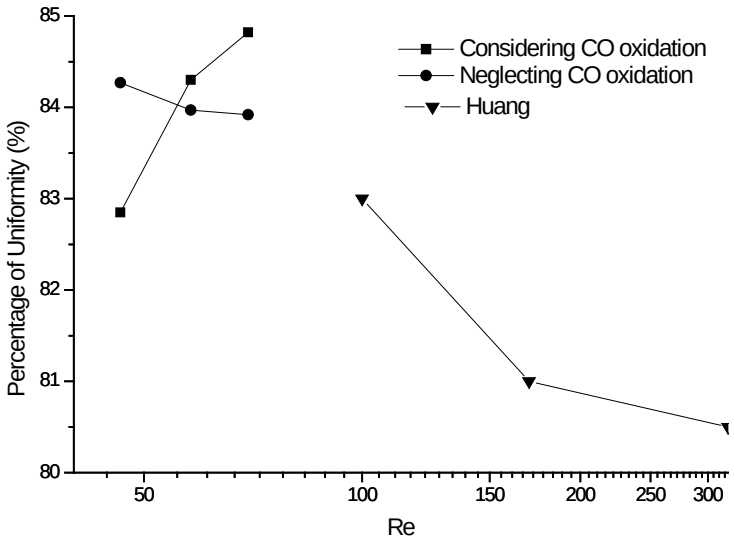


Fig.10. Degree of flow uniformity plotted against Re in this paper and Huang's work

Reynolds number is defined as:

$$\mathrm{Re} = \frac{\rho u d}{\mu} \tag{55}$$

where $u$ is the average velocity at the fuel channel inlet; $d$ is the fuel channel inlet width and $\mu$ is the dynamic viscosity of the fuel.

As can been seen from Fig.10, when neglecting CO oxidation, the percentage of uniformity decreases when Re increases, which is in accord with Huang's conclusion. However, when considering CO oxidation, the percentage of uniformity increases when Re increases. which is opposite to Huang's conclusion. Therefore, the CO oxidation has a significant influence on fuel velocity distribution nonuniformity among channels and should be considered when studying the fuel velocity distribution nonuniformity among channels.

## 4. Conclusions

In this paper, a comprehensive three-dimensional mechanistic model of an anode-supported SOFC unit was presented. The model coupled the intricate process of mass transfer, heat transfer, momentum transfer, reaction, electrochemical reaction, ionic conduction and electronic conduction to predict nonuniform flow velocity distribution among channels. A planar SOFC unit model with real cell geometry was developed by coupling heat and momentum transfer with a validated electrochemical model. A nonuniformity index was proposed to evaluate and compare fuel velocity distribution nonuniformity among channels in different working conditions. Effect of fuel velocity nonunifomtiy among channels on cell performance and effects of working condition such as working voltage, flow rate, flow-pattern and fuel type on fuel velocity distribution nonuniformity among channels were numerically investigated. The results were compared with similar study.

It was found that an increase in fuel velocity distribution nonuniformity among channels could lead to a decrease in cell performance and an increase in maximum local thermal stress. It was also found that the fuel velocity distribution was less uniform with lower working voltage, lower flow rate, using co-flow configuration instead of counter-flow or using syngas as fuel instead of hydrogen. Therefore, when designing a SOFC fuel channel, if the cell unit is supposed to work under low cell voltage or low flow rate, the channel designers should pay extra attention to the fuel velocity distribution nonuniformity among channels. Also, when choosing flow pattern or fuel type, fuel distribution nonuniformity should be a selection criterion. In addition, CO oxidation should not be neglected when studying fuel velocity distribution nonuniformity among channels. The paper provided a tool to quantitatively measure and compare degrees of fuel velocity distribution nonuniformity among channels in a SOFC unit in different working conditions.

**Acknowledgement**

This research was supported by the project 51106085 supported by National Natural Science Foundation of China and a grant (Project Number: PolyU5326/12E) from Research Grant Council, University Grants Committee, Hong Kong SAR.

**Reference:**

[1] Singhal SC. Solid oxide fuel cells for stationary, mobile, and military applications. J Solid State Ionics 2002;152:405-10.
[2] Singhal SC, Kendall K. High temperature solid oxide fuel cells: fundamentals, design and applications. New York:Elsevier;2003.
[3] Dey T, Ghosh PC, Singdeo D, Bose M, Basu RN. Diagnosis of scale up issues associated with planar solid oxide fuel cells. Int J Hydrogen Energy 2001;36:9967-76.
[4] Huang CM, Shy SS, Lee CH. On flow uniformity in various interconnects and its influence to cell performance of planar SOFC. J Power Sources 2008;183:205-13.
[5] Bi WX, Chen DF, Lin ZJ. A key geometric parameter for the flow uniformity in planar solid fuel cell stacks. Int J Hydrogen Energy 2009;34: 3873-84.
[6] Huang CM, Shy SS, Li HH, Lee CH. The impact of flow distributors on the performance of planar solid oxide fuel cell. J Power Sources 2010;195:6280-6.
[7] Liu H, Li P. Even distribution/dividing of single-phase fluids by symmetric bifurcation of flow channels. Int J Heat Fluid Flow 2013;40:165-79.
[8] Wang HJ, Shi YX, Cai NS. Numerical simulation of multi-channel planar solid oxide fuel cell unit by integrating continuum micro-scale PEN sub-model. ECS Trans 2011;35:1065-75.
[9] Minh NQ, Takahashi T. Science and technology of ceramic fuel cell. Amsterdam:Elsevier;1995.
[10] Loselevich AS, Kornyshev AA. Phenomenological theory of solid oxide fuel cell anode. J Fuel Cells 2001;1:40-65.
[11] Autissier N, Larrain D, van Herle J, Favrat D. CFD simulation tool for solid oxide fuel cells. J Power Sources 2004;131:313-9.

[12] Ni M. Modeling of SOFC running on partially pre-reformed gas mixture. Int J Hydrogen Energy 2012;37:1731-45.
[13] Costamagna P, Costa P, Antonucci V. Micro-modelling of solid oxide fuel cell electrodes. J Electrochim Acta 1998;43:375-94.
[14] Suwanwarangkul R. Model development and validation of solid oxide fuel cells using $H_2$-$H_2O$-CO-$CO_2$ mixtures: from button cell experiments to tubular and planar Cells. PhD thesis, Chemical Engineering, University of Waterloo, Waterloo; 2005.
[15] Krishna R, Wesselingh JA. The Maxwell-Stefan approach to mass transfer. Chem Eng Sci 1997;52:861-911.
[16] Fuller EN, Schettler PD, Giddings JC. New method for prediction of binary gas-phase diffusion coefficients. Ind Eng Chem 1966;58:18-27.
[17] Haberman BA, Young JB. Three-dimensional simulation of chemically reacting gas flows in the porous support structure of an integrated-planar solid oxide fuel cell. Int J Heat Mass Transfer 2004;47:3617-29.
[18] Shi YX. Modeling research on solid oxide fuel cells and SOFC-based hybrid systems. PhD thesis, Thermal Engineering, Tsinghua University, Beijing; 2008.
[19] Shi YX, Cai NS, Li C. Numerical modeling of an anode-supported SOFC button cell considering anodic surface diffusion. J Power Sources 2007;164:639-48.